# Diameter dependent threshold voltage modification of resistive state switching in organometallic single nanowire devices (diameter ∼ 10–100 nm)

Rabaya Basori[a),b)] and Sudeshna Samanta[c)]
*Unit for Nanosciences, Department of Condensed Matter Physics and Material Sciences, S. N. Bose National Centre for Basic Sciences, Kolkata 700106, India*



(Received 8 April 2018; accepted 25 August 2018; published online 21 September 2018)

Reversible electrical resistive state switching (ERSS) and memory effects have been investigated for a wide range of organometallic compounds and device configurations where the underlying mechanism is still not fully explored. We synthesized single nanowires (NWs) of organometallic charge transfer complexes between pre-fabricated electrodes with diameter ($d$) $10 \leq d \leq 100$ nm, and their ERSS properties have been systematically investigated at 300 K, encompassing versatile measurement techniques. The thinnest NW with $d \sim 10$ nm switched to its low resistive state with very low applied voltage. It appeared as metallic in the switched state as confirmed by its current-voltage characteristics and temperature ($T$) dependent resistivity for $100 \leq T \leq 300$ K. Supported by a theoretically simulated model, we proposed a possible mechanism for the single metallic filament formation in an almost defect-free 10 nm wire in its switched state considering the migration of metal ions created by a strong electric field between two very closely spaced electrodes. We also experimentally demonstrated that the diameter dependence of the threshold voltage ($V_{th}$) for switching follows a power law ($V_{th} \propto d^{\delta}$) which is independent of the electrode configurations, measurement techniques and growth mechanism. The results explained the strategies to engineer the ERSS properties of single NW devices and might be beneficial for further research and development. *Published by AIP Publishing*. https://doi.org/10.1063/1.5033970

Microelectronics deals with the miniaturization of integrated circuits (ICs), and its evolution resulted in complex system-on-a-chip devices. Over time, an increased integrity of the transistors in a reduced area of an IC has been achieved by the continuous downscaling of semiconductor devices. Such downscaling already approached the physical and technological limit of the feature size of an IC, and further downscaling became restricted for many of those device components.

Random access memory (RAM) is one of the most important parts of an IC in recent data processing and storage technology. Due to the versatile working principles, (i) ferroelectric-RAM (FeRAM), (ii) magnetoresistive-RAM (MRAM), and (iii) phase-change-RAM (PRAM) received great attention for next-generation nonvolatile memories. Recently, a promising candidate has emerged as a resistance-RAM (ReRAM) exhibiting resistive state switching properties and is based on metal oxides[1,2] and organic compounds[3,4] (supplementary material). Due to diversity, tailorability, multifunctionality, and having conjugated structures composed of small molecules, the organometallic charge transfer complexes were found as very good ReRAM materials over the last few decades.[5–7] They are very well known for their electrical resistive state switching (ERSS) with large applications in ReRAM or memory resistor (MEMRISTOR).[8] The materials received considerable interest due to their potential applications as humidity sensors[9] and high responsivity photo-detectors.[10] To use a device as ReRAM or MEMRISTOR for industrial applications will prefer a switching material having a high ON/OFF current ratio to distinguish between two distinct states ("1"/"0"), large cycling endurance to increase its lifetime, and a low threshold field of switching for low power consumption. CuTCNQ (Copper 7,7,8,8-tetracyanoquinodimethane) is one of the charge transfer organometallic compounds which has reversible bistable ERSS.[7] The switching phenomenon of the same was explained with the filament formation by the redox reaction in detail.[5,6,11,12] Similarly, the electrode material dependent switching[13] and length ($l$) dependent threshold voltage ($V_{th}$) for switching[14] along with its opto-electronic control[15] have been studied earlier. However, the electrical switching by field dependent self-multiplication of the charge carriers in the nanowire was explained without any experimental evidence.[14]

Considering the results of the length-dependent $V_{th}$ of a single nanowire (SNW) device and requirement for a low $V_{th}$ for industrial applications, we found that $V_{th}$ can be significantly tuned by the NW diameter ($d$). In this article, we tried to attend few fundamental questions as follows: (a) does the threshold field $E_{th}$ (electric field corresponding to $V_{th}$) depend on $d$? (b) if yes, the nature of the dependency and possible reasons for the same, and finally, (c) does there exist any limiting value of $d$ for ERSS to appear in a SNW device?

In a Wigner crystal type polymeric NW, $E_{th}$ follows an inverse power law with $d$ at low temperatures,[16] whereas $V_{th}$ is inversely proportional to $d$ in a NW field effect transistor (NWFET) due to the greater influence of the surface scattering processes.[17,18] In this article, we experimentally demonstrated the ERSS phenomena in CuTCNQ NWs for 10

[a)]Present address: School of Nanoscience and Technology, Indian Institute of Technology, Kharagpur 721302, India.
[b)]Email: rabaya@iitkgp.ac.in.
[c)]Present address: Center for High Pressure Science and Technology Advanced Research, Shanghai 201203, China.

$\leq d \leq 100$ nm where we showed that $E_{th}$ followed a power law dependence with $d$. We also investigated that such a phenomenon was independent of any measurement and device fabrication process and solely related to the intrinsic properties of the NWs. Any study of the diameter dependence of the threshold field modification in SNWs of a charge transfer complex has not been reported earlier.

CuTCNQ NWs of diameter 10–100 nm were grown by the physical vapour deposition (PVD) method by reacting TCNQ vapour with Cu at $\simeq$120–130 °C. The details of characterization (XRD, FTIR, and Raman spectroscopy, and HRTEM) are elaborated in the supplementary material. To demonstrate that the diameter dependence of $E_{th}$ is an intrinsic property of the material and is independent of the device fabrication processes as stated earlier, we fabricated SNW devices by two mutually orthogonal approaches, i.e., bottom-up and top-down approaches. The SEM images of the SNW devices grown by bottom-up and top-down approaches are shown in Figs. 1(a) and 1(b), respectively, by down arrows. (Details of growth, characterization, and device fabrication are described in the supplementary material.) We followed different experimental techniques to study ERSS and came to a conclusion that switching behaviour is independent of the measurement routes. We performed electrical measurements on three different types of systems: CuTCNQ SNWs connected with electrical contact pads (i) developed by electron beam lithography (EBL) as the *bottom-up* approach [Fig. 2(a)]; (ii) by deposition of Pt using focused electron and ion beam (FEB and FIB) as the *top-down* approach [Fig. 2(b)], and (iii) the CuTCNQ NW film. ERSS and temperature-dependent resistivity experiments were carried out with direct-current (d.c) and alternating current (a.c) techniques, respectively. Conducting Atomic Force Microscopy (c-AFM) was utilized for electrical characterization of the CuTCNQ NW film where the device construction is schematically demonstrated in the inset of Fig. 2(c). We followed a two-probe configuration to observe ERSS and temperature ($T$) dependent electrical resistivity ($\rho$).

In order to better predict the behaviour of the devices, two terminal $I$–$V$ characteristics were taken in five individual SNW devices with varying $d$ and $l$. To eliminate

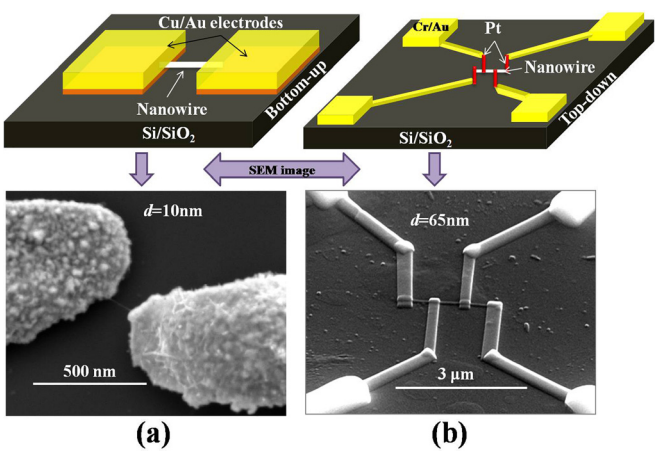


FIG. 1. Schematic representation of bottom-up and top-down approaches. The SEM image of the PVD grown CuTCNQ SNW device: (a) $d \sim 10$ nm and $l \sim 200$ nm connected between two e-beam lithographically patterned Cu/Au electrodes and (b) $d \sim 65$ nm and $l \sim 2.5\mu$m connected with four FEB deposited Pt electrodes.

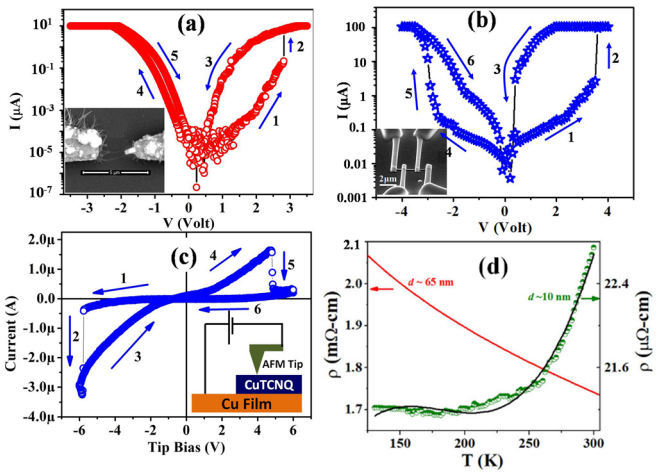


FIG. 2. $I$–$V$ characteristics with ERSS of different SNW devices with varying $d$: (a) $d \sim 70$ nm (pre-fabricated Cu/Au electrodes) and (b) $d \sim 65$ nm (FEB deposited Pt). Insets show the SEM images of respective devices. (c) $d \sim 40$ nm measured with the conducting AFM tip as the top electrode where the inset shows a schematic illustration. (d) Comparison of $\rho$ vs. $T$ data of SNWs having diameters 65 nm and 10 nm, showing semiconducting and metallic behaviours, respectively.

the geometrical dependence of our devices, we considered three different geometrical arrangements for $I$–$V$ measurements: (i) two lateral grown with two different approaches (top-down and bottom-up) and (ii) one vertical arrangement (using the c-AFM setup). The dimension of the SNW device also varies from $\sim$10–70 nm in diameter and $\sim$200 nm–5 $\mu$m in length between two electrodes. Figure 2(a) shows $I$–$V$ data for a SNW device of $d \sim 70$ nm made by the bottom-up approach which showed switching from the high-resistive state (HRS) to the low-resistive state (LRS) for $V_{th}$ of $\sim$3 V. Another SNW device fabricated by the top-down approach of $d \sim 65$ nm showed ERSS for $V_{th} \sim 3.6$ V as shown in Fig. 2(b). ERSS had also been observed in a SNW grown on the Cu film where $I$–$V$ data were recorded between the Cu film as the bottom electrode and approaching a c-AFM tip on the individual NW as the top electrode, which is shown in Fig. 2(c). During the measurement with the AFM tip, we used a variable gain FEMTO amplifier (supplied with the VEECO AFM) and an electrometer where a schematic of the same is shown in the inset of Fig. 2(c). Irrespective of the three different NW diameters, geometries, and fabrication methods of the individual devices, the corresponding $I$–$V$ characteristics of the NWs showed that switching $E_{th}$ is within the range of $\sim 10^5$–$10^7$ V/m. Generally, the CuTCNQ NW is semiconducting in nature, but surprisingly, our device of diameter 10 nm [SEM image in Fig. 1(a)] appeared as metallic type as found from the $\rho - T$ characteristics shown in Fig. 2(d). $\rho$ for the 10 nm NW is about three-times lower than the resistivity of the 65 nm NW at 300 K.

To avoid any sudden collapse of the 10 nm thin NW, it is always safe to calculate the current density ($J$) as it increases sharply with decreasing $d$ ($J \propto 1/d^2$). The calculated $J$ values for our different SNW devices in the switched state (LRS) were lying within the range of $\sim 10^5$–$10^6$ A/cm$^2$ which were slightly higher compared to the devices reported earlier[14,19] represented by the solid circles in Fig. 3(a). Hence, we conclude that the range of $J$ values was in a safe

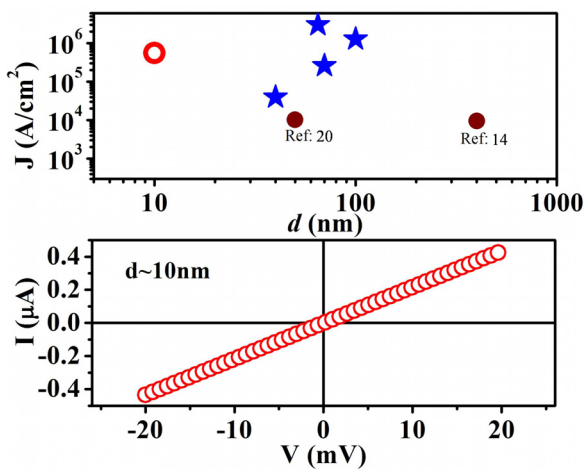


FIG. 3. (a) Variation of $J$ with $d$ in LRS. Blue stars and red circles are for devices with 40 nm $\leq d \leq$ 100 nm and $d \sim$ 10 nm, respectively. Solid circles are the results from earlier reports. (b) $I$–$V$ data for the 10 nm SNW device at 300 K.

region for CuTCNQ NWs and would not be destroyed due to power dissipation as all our devices sustained for a large $J \sim 10^6$ A/cm$^2$. Hence, to achieve $J$ for the 10 nm SNW device to get it in the switched state, we passed a maximum current of ~0.43 $\mu$A and measured $\rho - T$ with that constant current. As expected, $\rho - T$ shows metallic behaviour as shown in Fig. 2(d) which was also confirmed from the linear $I$–$V$ plot as depicted in Fig. 3(b).

We have plotted $E_{th}$ as a function of the NW diameter (40 nm $\leq d \leq$ 400 nm) in Fig. 4 and fitted with $E_{th} \propto d^{\delta}$ with $\delta \sim 1.4$ (solid line). This dependence of $E_{th}$ on the diameter also matches well with the value of threshold fields previously reported by other groups.[14,19] We extrapolated this fit to a lower diameter as ~10 nm, and we could estimate $E_{th} \sim 10^5$ V/m for a NW of $d \sim$ 10 nm and length ~ 200 nm. Thus, voltage applied across the 10 nm wire (20 mV, corresponding field ~ $10^5$ V/m) brought the system to its switched state, and NWs showed ohmic behaviour as shown in Fig. 3(b).

The proposed physical mechanisms responsible for ERSS are diverse, and mechanisms such as highly localized filamentary conduction,[20,21] change in the number of free carriers by charge transfer in donor-acceptor complexes,[22] or inherent electronic molecule[23] are often used for explanation. Switching occurs because of the formation of a metallic channel at the interface between the NWs and the electrodes.[7] The mechanism involved for the same is strongly dependent on the work function of electrodes connecting the NWs and the device structure.[13] The NW device connected with high work function materials such as Pt, Au, and Mo shows regular switching, whereas electrodes with low work function materials such as Al, In, and Zr show inverse switching. In regular switching, system switches from HRS to LRS for applied positive bias, and in inverse switching, HRS to LRS switching occurs for negative applied bias. In this report, single NW devices connected with Au and FEB deposited Pt as shown in Figs. 2(a) and 2(b), respectively, exhibited regular switching, whereas the NW device connected with Al exhibited inverse switching as shown in Fig. 2(c). Reduction and oxidation of the Cu ions from the CuTCNQ NW and Cu electrodes lead to the formation and rupture of the Cu metallic channel at the interface of NWs and top electrodes caused the transition from HRS to LRS and vice versa.

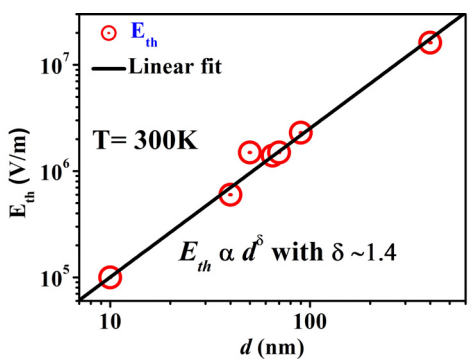


FIG. 4. Variation of $E_{th}$ with $d$ for SNW devices at 300 K (includes data from Refs. 14 and 19). The solid line shows a power law fit $E_{th} \propto d^{\delta}$ with $\delta \sim 1.4$.

In our case, the diameter dependence of $E_{th}$ can be explained considering the existence of excessive copper ions, other impurities or defects such as charged solitons, or neutral-ionic domain inside the NW during growth and fabrication.[24] How these excessive copper ions formed filament like structures between the NW and electrodes responsible for ERSS and mediated the charge transfer from electrodes to CuTCNQ is shown in Fig. 5. This model is based on the migration of the metal ions inside the electric field. When a positive bias voltage between the two electrodes was applied, it created a strong electric field as simulated by COMSOL Multiphysics simulation software shown in Fig. 5(a). The arrows denoted the direction of the electric field. The strong electric field caused the oxidation of the electrode metal Cu. The resulting $Cu^{++}$-ions were mobile and drifted due to the electrical field towards the cathode. These cations reached the negatively charged counter electrode, leading to the growth of Cu filaments as shown schematically in Fig. 5(b). The filaments were highly conducting, and the NW was in a low-resistive ON state. During the filamentary conduction process, as the Joule heat is dissipated by low resistive thick electrodes or Joule heating itself is low at the NW, the conductive filaments do not get destroyed and continue in the LRS state. If a negative bias voltage was applied to the copper electrode, an electrochemical dissolution of the same conductive bridges took place, leading the system into a high-resistive OFF state. Cu had good electrochemical mobility, and hence, it is often used as an electrode material. There could also be possibility of the formation of partial metals Cu and $Cu_xO$ supported by photoemission electron microscopy.[25] Moreover, the transport properties associated

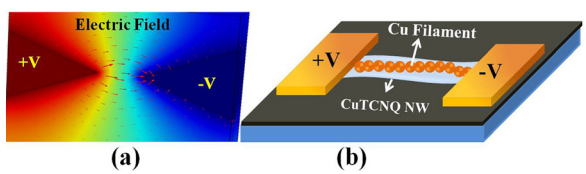


FIG. 5. (a) Distribution of $E$ between two electrodes (color code → magnitude and arrow → direction) by COMSOL Multiphysics. (b) Schematic of filament formation by Cu ions in SNWs.

with charge transfer depend on various quantities such as migration of mobile defects and oxygen vacancies, tunnelling rates, the number of states in the ionic domains, transition probabilities, and their occupations in the states.

In general, the density of defect states increases in NWs of larger diameter and energy required to transfer the system into a switched LRS is high. The defect state density decreases with the decrease in $d$, and hence, required energy to fill the available energy states also decreases. This explains the reduced $E_{th}$ of switching with decreasing NW diameter as reflected in our experimental results (see Fig. 3). When $d$ is low as $\sim$10 nm, it became almost a defect free NW with a high concentration of Cu ions within a small length of $\sim$200 nm. The small distance between the two electrodes created a very high $E_{th}$ at low bias and was sufficient to bring the low-dimensional NW almost a defect-free NW at its switched state. The 10 nm NW might appeared as a single Cu filament attached to the electrodes which made the system metallic. A single filament formation scenario could be reasonable because the first conducting filament could reduce $E_{th}$ across the NW and hence restricted the multiple filament formation. For simplicity, we can consider a pure single filament model to reveal the basic operational principle, and the overall resistance ($R$) at the ON state can be written as

$$R = \Sigma_{k=1}^{N} R_{m,k} + \Sigma_{k=1}^{N} R_{T,k}, \tag{1}$$

where $R_{m,k}$ and $R_{T,k}$ denote the contributions from resistance from metallic grains and tunnel resistance in series, respectively. Considering the temperature dependence response of $R$, we can rewrite Eq. (1) as

$$R(T) = \Sigma_{k=1}^{N} R_{m,k}^{T_0}[1 + \alpha(T - T_0)] + \Sigma_{k=1}^{N} R_{T,k}^{0} \frac{\sin(C_k T)}{C_k T}, \tag{2}$$

where $R_{m,k}^{T_0}$ is the resistance of each metal grain at temperature $T_0$, $\alpha$ is the temperature coefficient of metallic Cu, $R_{T,k}^{0}$ is the tunnel resistance at $T = 0$, and $C_k$ is a geometric constant depending on the tunneling distance $\xi$ and barrier potentials at contacts.

We can assume that all the metallic grains are equidistant from each other, and hence, $C_k$ can be the same for every grain gap. The simplified equation can be written as follows:

$$R(T) = R_m^{T_0}[1 + \alpha(T - T_0)] + R_T^0 \frac{\sin(CT)}{CT}, \tag{3}$$

where $R_m^{T_0}$ is the total resistance of the Cu filament at temperature $T_0$ and $R_T^0$ is the overall tunnel resistance at $T = 0$. For Cu, $\alpha = 3 \times 10^{-3}\ \mathrm{K}^{-1}$, and we took $T_0 = 300$ K. The temperature dependence of $R$ could be qualitatively fitted using Eq. (3) with $R_m^{T_0} = 620\,\Omega$, $R_T^0 = 498\,\Omega$, and $C = 0.01146\,\mathrm{K}^{-1}$, shown by the solid line in Fig. 2(d). The low value of $R_m^{T_0}$ again confirms the quality of the NW and validates our filament formation scenario. The estimated filament resistivity $\rho_M^{T_0}$ is 23 $\mu\Omega$ cm which is one order higher than the bulk resistivity of Cu $\sim 1.68\,\mu\Omega$ cm at 300 K. Our results postulate a probable mechanism to achieve a permanently switched metallic state in a thin SNW of $d \simeq 10$ nm [Fig. 2(d)]. Moreover, Fig. 4 might help to estimate $V_{th}$ for a SNW with a known diameter, before performing any switching experiment. Unfortunately, we observed that the size reduction in such a NW actually did not help much, and the loss of ERSS even at very low applied voltage was not advantageous at all.

In conclusion, we have measured electrical resistive state switching of SNW devices with a diameter ranging from 10 nm to 100 nm adopting versatile techniques. The threshold field of switching follows a power law dependence on the diameters of the nanowire which is independent of the electrode configuration, measurement techniques, and growth mechanism. Our study roughly predicts the correct diameter selection of an organometallic NW device to observe the ERSS prior to the measurements. For the nanowire with smallest diameter ($d \sim 10$ nm), we proposed the model of metallic filament formation by Cu ions between two closely spaced electrodes. We observed that the device lost its ERSS property and hence restricts its application to memory devices. Finally, we conclude that the growing interest in miniaturization of circuit elements with such a one-dimensional nanostructured material sometimes may not be a viable route from an application point of view.

See supplementary material for comparison of the CuTCNQ ERSS property with binary oxides, material synthesis, device fabrication, characterization, and retention properties.

R.B. and S.S. thank DST (UNANST-II), Nanomission, Government of India (Ref. No. SR/NM/NS-53/2010). R.B. acknowledges the project [DST/INSPIRE Faculty Award/2016/DST/INSPIRE/04/2015/003152] funded by DST, Government of India, for partial manpower support. R.B. and S.S. thank Professor A. K. R. for valuable suggestions and instrumental facilities.

[1]C.-H. Huang, W.-C. Chang, J.-S. Huang, S.-M. Lin, and Y.-L. Chueh, Nanoscale **9**, 6920–6928 (2017).
[2]H. Du, T. Wan, B. Qu, F. Cao, Q. Lin, N. Chen, X. Lin, and D. Chu, ACS Appl. Mater. Interfaces **9**, 20762–20770 (2017).
[3]D. Chaudhary, S. Munjal, N. Khare, and V. D. Vankar, Carbon **130**, 553–558 (2018).
[4]Y. Xin, X. Zhao, X. Jiang, Q. Yang, J. Huang, S. Wang, R. Zheng, C. Wang, and Y. Hou, RSC Adv. **8**, 6878–6886 (2018).
[5]R. S. Potember, T. O. Poehler, and D. O. Cowan, Appl. Phys. Lett. **34**, 405 (1979).
[6]J. Billen, S. Steudel, R. Mller, J. Genoe, and P. Heremans, Appl. Phys. Lett. **91**, 263507 (2007).
[7]R. Basori, M. Kumar, and A. K. Raychaudhuri, Sci. Rep. **6**, 26764 (2016).
[8]R. Müller, S. D. Jonge, K. Myny, D. J. Wouters, J. Genoe, and P. Heremans, Appl. Phys. Lett. **89**, 223501 (2006).
[9]K. Wang, X. Qian, L. Zhang, Y. Li, and H. Liu, ACS Appl. Mater. Interfaces **5**, 5825–5831 (2013).
[10]R. Basori, K. Das, P. Kumar, K. S. Narayan, and A. K. Raychaudhuri, Opt. Express **22**, 4944–4952 (2014).
[11]D. Deleruyelle, C. Muller, J. Amouroux, and R. Müller, Appl. Phys. Lett. **96**, 263504 (2010).
[12]J. G. Simmons, Phys. Rev. **155**, 657–660 (1967).
[13]A. Hefczyc, L. Beckmann, E. Becker, H.-H. Johannes, and W. Kowalsky, Phys. Status Solidi (a) **205**, 647–655 (2008).
[14]K. B. Zheng, H. T. Shen, C. N. Ye, J. L. Li, D. L. Sun, and G. R. Chen, Nano-Micro Lett. **1**, 23–26 (2009).
[15]R. Basori and A. K. Raychaudhuri, Nano-Micro Lett. **6**, 63–69 (2014).

[16]A. Rahman and M. K. Sanyal, Phys. Rev. B **76**, 045110 (2007).
[17]B.-M. Nguyen, Y. Taur, S. T. Picraux, and S. A. Dayeh, Nano Lett. **14**, 585–591 (2014).
[18]K. Kim, P. C. Debnath, D.-H. Park, S. Kim, and S. Y. Lee, Appl. Phys. Lett. **96**, 083103 (2010).
[19]K. Xiao, I. N. Ivanov, A. A. Puretzky, Z. Liu, and D. B. Geohegan, Adv. Mater. **18**, 2184–2188 (2006).
[20]R. Basori, K. Das, P. Kumar, K. S. Narayan, and A. K. Raychaudhuri, Appl. Phys. Lett. **102**, 061111-4 (2013).
[21]H. Pagnia and N. Sotnik, Phys. Status Solidi (a) **108**, 11–65 (1988).
[22]M. Lauters, B. McCarthy, D. Sarid, and G. E. Jabbour, Appl. Phys. Lett. **89**, 013507-1-3 (2006).
[23]Z. K. Keane, J. W. Ciszek, J. M. Tour, and D. Natelson, Nano Lett. **6**, 1518–1521 (2006).
[24]Y. Iwasa, T. Koda, Y. Tokura, S. Koshihsra, N. Iwssawa, and G. Saito, Appl. Phys. Lett. **55**, 2111–2113 (1989).
[25]R. Yasuhara, K. Fujiwara, K. Horiba, H. Kumigashira, M. Kotsugi, O. Oshima, and H. Takagi, Appl. Phys. Lett. **95**, 012110 (2009).